Journal of the European Ceramic Society 23 (2003) 887–896

www.elsevier.com/locate/jeurceramsoc

Sintering and mass transport features of $(Sn,Ti)O_2$ polycrystalline ceramics

P.R. Bueno[a,*], E.R. Leite[a], L.O.S. Bulhões[a], E. Longo[a], C.O. Paiva-Santos[b]

[a] *Universidade Federal de São Carlos, C.P. 676, CEP 13565-905, São Carlos, SP, Brazil*
[b] *Universidade Estadual de São Paulo, C.P. 335, CEP 14800-900, Araraquara, SP, Brazil*

Received 28 November 2001; received in revised form 12 June 2002; accepted 30 June 2002

Abstract

Different $(Sn,Ti)O_2$ compositions were sintered at 1450 °C for 2 h with the purpose of investigating their sintering and mass transport properties. Highly dense ceramics were obtained and their structural properties studied by X-ray diffraction and scanning electron microscopy. The changes in lattice parameters were analyzed by the Rietveld method and two mass transport mechanisms were observed during sintering in different temperature ranges, evidenced by the linear shrinkage rate as a function of temperature. The effect of the concentration of TiO_2 on mass transport and densification during sintering was analyzed by considering the intrinsic defects. System densification was attributed to a mass transport mechanism in the SnO_2 matrix, caused by the presence of TiO_2, which formed a solid solution phase. The change in the mass transport mechanism was attributed to chemical bonding between SnO_2 and TiO_2, which improves ionic diffusion as the concentration of TiO_2 increased in $(Sn,Ti)O_2$ compositions.

Keywords: Microstructure-final; Sintering; $(Sn,Ti)O_2$

1. Introduction

Tin dioxide is an *n* type semiconductor with a tetragonal crystalline structure similar to that of the rutile structure.[1] This material has been used in a great number of technological applications such as gas sensors, electrocatalytic electrodes, electro-optical devices and in photovoltaic cells.[1–9] High voltage SnO_2 varistors have recently been developed based on this oxide.[10] Most SnO_2 applications have employed porous ceramic structures (gas sensor) or thin films[11–13] (mainly for electronic and electrochemical applications).

The electrical properties of low density SnO_2 polycrystalline ceramics depend on the non-stoichiometry of the oxide surface, the powder preparation method, the temperature, and the atmosphere used during thermal treatment. This dependence on non-stoichiometry is related to poor densification.[2–9] Because of this poor SnO_2 densification, most of its applications are based on the high specific surface area presented by components. Low densification is believed to be caused by the predominance of non-densifying mechanisms, such as the evaporation–condensation process and surface diffusion.[14] These mechanisms are responsible for grain growth and the formation of necks between particles during sintering but do not promote densification. Thus, devices based on SnO_2 have a porosity of up to 40%, which is very desirable for gas sensor applications, but is undesirable in applications requiring mechanical strength.

Like SnO_2, TiO_2 in the rutile phase is an electrically conductive ceramic (as well as an n-type semiconductor) material with a tetragonal crystalline structure. TiO_2 is being investigated for applications in electrocatalysis, photoelectrochemistry and as a counter electrode in smart windows.[15] When fully dense, TiO_2 displays properties similar to those observed in SnO_2 for low voltage varistors[16] and humidity sensors.[7] TiO_2 differs from SnO_2 during sintering because, unlike SnO_2, no dopants are required to densify it. Densities close to the theoretical[16] values are achieved by sintering at around 1300 °C.

* Corresponding author.
E-mail address: paulo@iris.ufscar.br (P.R. Bueno).

0955-2219/03/$ - see front matter
PII: S0955-2219(02)00234-0

The thermodynamic and kinetic properties of isostructural solid solutions between SnO_2 and TiO_2 have been quite extensively studied. However, more general properties relevant to applications of SnO_2–TiO_2 binary compositions have not yet been investigated in depth. The crystallographic and thermodynamic properties of the SnO_2–TiO_2 system have been exhaustively investigated to determine the phase diagram[17–25] and to study the extent of spinodal decomposition. Fig. 1 presents a schematic representation of the phase diagram for the solid state SnO_2-TiO_2 binary composition. This system shows a miscibility gap, such as that proposed by Schultz and Stubican,[17,18] Gupta and Cooper,[19] and Park et al.[20] Interest in spinodal decomposition began with Cahn's[26] classic work about the kinetics of spinodal decomposition in metallic binary systems. Since that time, experimental evidence of the occurrence of this type of phase separation has been published in the literature for a large number of systems, including metallic alloys of Al–Zn,[27] Au–Ni[28] and, later, in glasses[29] and ceramics. In crystalline materials, the characteristics of spinodal decomposition are modified by the elastic strain energy accompanying compositional separation. Due to the anisotropy of crystal elastic constants, composition waves tend to propagate in the interfaces parallel to elastically soft directions of the crystal, often resulting in lamellar structures. The SnO_2–TiO_2 system possesses a nearly symmetric miscibility gap (Fig. 1). Upon cooling a solid solution from a high temperature in the miscibility gap, a structure consisting of finely divided lamellae alternatively rich in Sn and Ti, is formed within each polycrystalline grain.[20–25]

Because the SnO_2–TiO_2 system offers one of the best example of spinodal decomposition in ceramics, the thermodynamic properties and the kinetics of spinodal decomposition in this system have been extensively studied.[20–25] However, solid solutions of SnO_2–TiO_2 systems have only recently emerged as attractive materials for application in electronic devices, particularly in gas sensor applications.[30,31] Radecka et al.[30] have studied the SnO_2–TiO_2 compositions for gas sensor applications[30] and have explored the transport properties[31] of polycrystalline ceramics and thin films. However, apart from this, little is known about the basic optical and electrical features of the (Sn,Ti)O_2 system and the answers to questions regarding mass transport, charge carriers and the sintering mechanism have not yet been found.

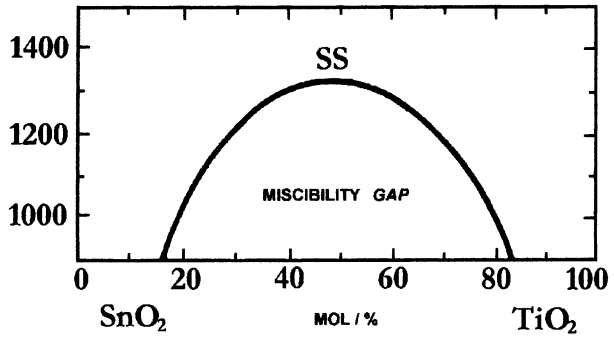

Fig. 1. Schematic representation of the SnO_2–TiO_2 phase.

In this work, we investigate the sintering parameters and some aspects of mass transport in (Sn,Ti)O_2 polycrystalline ceramics with different compositions prepared by a mechanical mixture of oxides, correlating them to the chemical bonding nature and the intrinsic structural defects of these polycrystalline ceramics.

2. Experimental procedure

(Sn, Ti)O_2 powders were prepared by mechanical mixing of SnO_2 and TiO_2 powders in isopropyl alcohol for 24 h, using polypropylene jars with yttrium stabilized zirconia balls to aid the mixing process. The oxides used were SnO_2 (Merck) and TiO_2 (Merck), both in analytical grade. The molar binary system compositions were 100% SnO_2 (SnO_2); 75.0% SnO_2 + 25.0% TiO_2 ($Sn_{0.75}Ti_{0.25}O_2$); 50.0% SnO_2 + 50.0% TiO_2 ($Sn_{0.50}Ti_{0.50}O_2$); 25.0% SnO_2 + 75.0% TiO_2 ($Sn_{0.25}Ti_{0.75}O_2$) and 100% TiO_2 (TiO_2). The specific surface area of the starting powder for the sintering process was obtained using the BET isotherm technique (Micromeritics Asap 2000).

After drying, the powders were pressed into pellets (11.0 mm × 1.0 mm) by uniaxial pressing (20 MPa), followed by isostatic pressing at 210 MPa. The pellets were then sintered at 1450 °C, using a heating rate of 10 °C/min for 2 h at ambient atmosphere, followed by cooling to room temperature at a rate of 10 °C/min. The grain size was determined by SEM (scanning electron microscopy) micrographic analysis (using a ZEISS microscope, model DSM 940A) and an image analysis software package (PGT—IMIX/ASTM-112 norm). The relative densities of the samples were measured using the Archimedes method. The lattice parameter, unit cell volume, density and phases of sintered samples were determined by X-ray diffraction patterns (obtained with a SIEMENS diffractometer, model D-5000, CuK_α radiation) and refined by the Rietveld method[32] using the DBWS-9411 program.[33]

Sintering was monitored with a Netzch 402E dilatometer at a constant heating rate of 10 °C/min in an ambient atmosphere.

3. Results and discussion

3.1. Structural characterization

The specific surface area of the starting powders was very similar. For pure SnO_2 and TiO_2, the areas were 9.2 and 9.8 m^2/g, respectively. For binary compositions

$Sn_{0.75}Ti_{0.25}O_2$, $Sn_{0.50}Ti_{0.50}O_2$ and $Sn_{0.25}Ti_{0.75}O_2$ the areas were, respectively, 10.3, 10.1 and 10.8 m^2/g. Thus, the sintering process could be examined without taking into account the initial specific surface area.

Fig. 2 shows the SnO_2 and TiO_2 structures after sintering at 1450 °C for 2 h in an ambient atmosphere. As expected, SnO_2 presented a lower relative density (60.5% of the theoretical density), while TiO_2 showed a higher density (90.3% of the theoretical density) under the sintering conditions employed.

Figs. 3–5 present the $Sn_{0.75}Ti_{0.25}O_2$, $Sn_{0.50}Ti_{0.50}O_2$ and $Sn_{0.25}Ti_{0.75}O_2$ SEM micrographs, also sintered at 1450 °C for 2 h in an ambient atmosphere. Table 1 presents the theoretical density, experimental density (from Rietveld refinement parameters) and relative density values (from sintered samples) for the pure and binary compositions.

It was observed that all the binary compositions presented higher relative density values than the pure SnO_2 and TiO_2 compositions. Moreover, there was an increase in the relative density values with an increase of TiO_2 concentration in the binary compositions. The higher densification values of SnO_2–TiO_2 compositions in comparison to the pure components are probably due to the higher mobility of interstitial and vacancy defects, enhancing mass transport. This feature is discussed further.

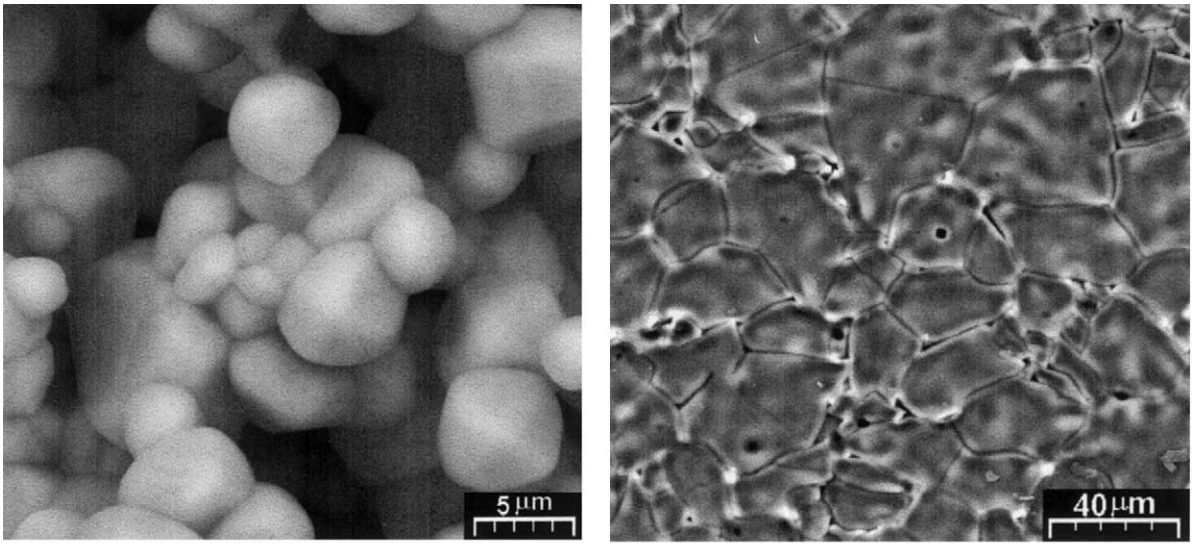

Fig. 2. SEM micrographs of pure (a) SnO_2 and (b) TiO_2 samples sintered at 1450 °C for 2 h in an ambient atmosphere, using a cooling rate of 10 °C min^{-1}.

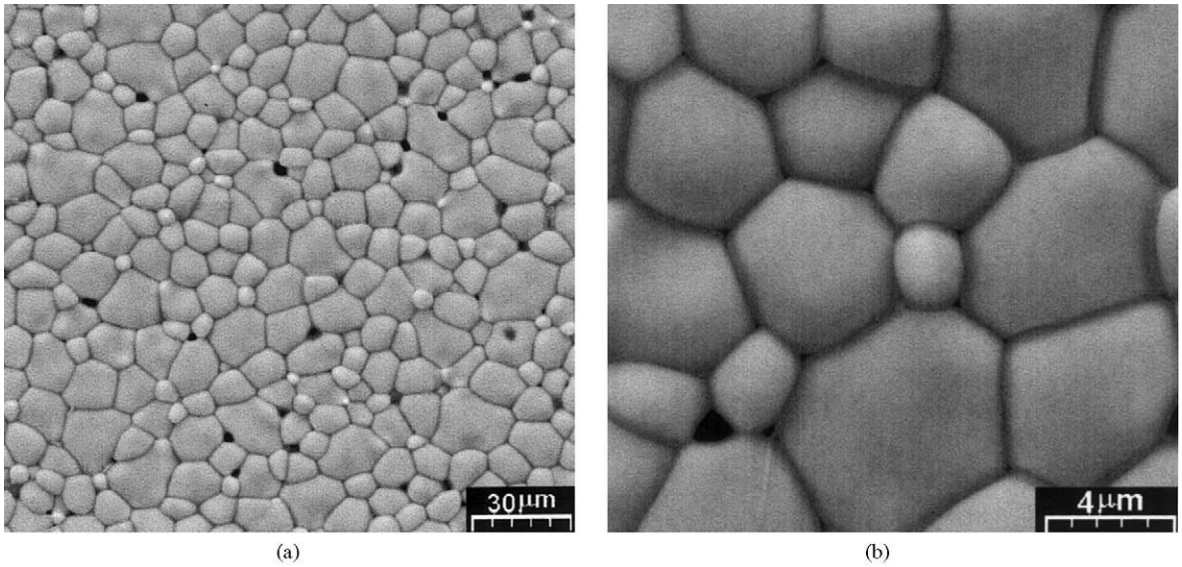

Fig. 3. SEM micrographs of $Sn_{0.75}Ti_{0.25}O_2$ composition samples sintered at 1450 °C for 2 h in an ambient atmosphere, using a cooling rate of 10 °C min^{-1}.

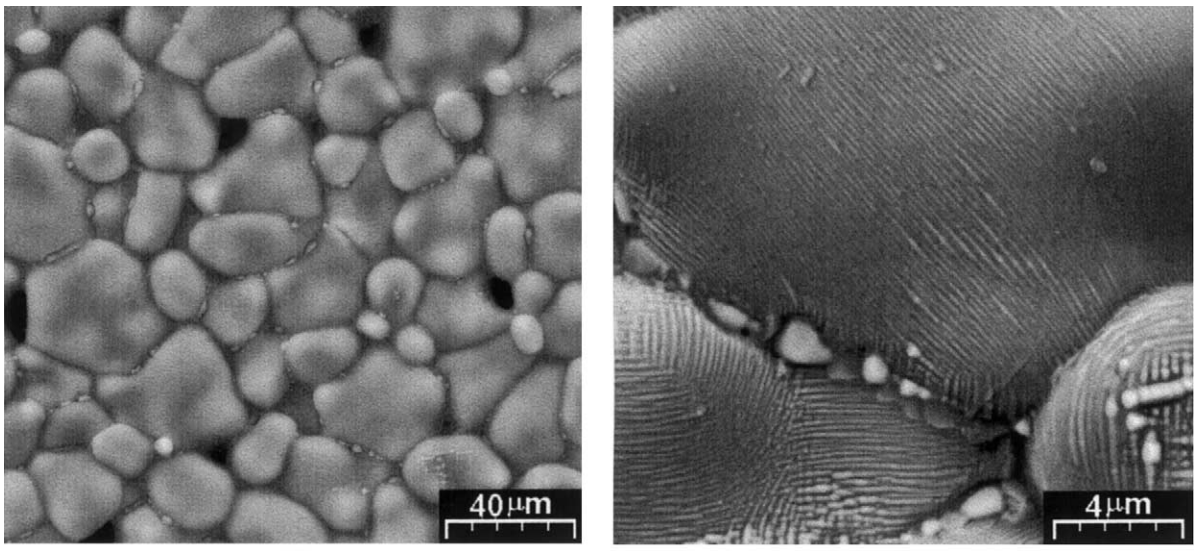

Fig. 4. SEM micrographs of $Sn_{0.50}Ti_{0.50}O_2$ composition samples sintered at 1450 °C for 2 h in an ambient atmosphere, using a cooling rate of 10 °C min^{-1}.

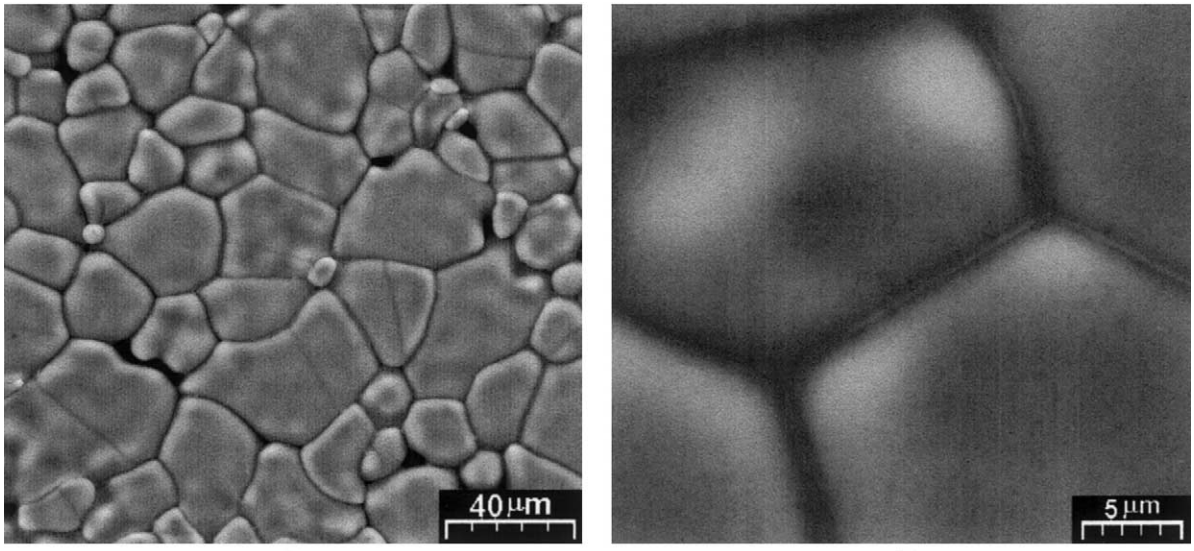

Fig. 5. SEM micrographs of $Sn_{0.25}Ti_{0.75}O_2$ composition. Samples sintered at 1450 °C for 2 h in an ambient atmosphere, using a cooling rate of 10 °C min^{-1}.

Table 1
Theoretical density, relative density (from sintered samples) and experimental density (from Rietveld refinement) values of pure and binary compositions

System	Theoretical density (g/cm^3)	Experimental density (g/cm^3)	Relative density (%)
SnO_2	6.99[a]	6.98 ±0.04	60.5
$Sn_{0.75}Ti_{0.25}O_2$	6.30	6.36 ±0.05	95.6
$Sn_{0.50}Ti_{0.50}O_2$	5.62	–	96.4
$Sn_{0.25}Ti_{0.75}O_2$	4.93	4.99 ±0.05	98.2
TiO_2	4.25[b]	4.24 ±0.03	94.5

[a] JCPDS-ICDD—No. 41–1445 (Quality: *).
[b] JCPDS-ICDD—No. 21–1276 (Quality: *).

Table 2 presents the lattice parameters of the pure and binary compositions obtained by structural refinement using the Rietveld method.[33] The values calculated by structural refinement differ by no more than 2% from the theoretical values, confirming the formation of a solid solution and completion of the reaction by the time the compositions had undergone the maximum temperature, except to the $Sn_{0.50}Ti_{0.50}O_2$ binary composition.

Fig. 6 illustrates the X-ray diffraction patterns of the pure and binary compositions. The formation of a solid solution was observed even when a higher concentration of TiO_2 was present in the SnO_2 lattice ($Sn_{0.75}Ti_{0.25}O_2$).

Table 2
Lattice parameter values of pure and binary compositions obtained through structure refinement using the Rietveld method

System	a Lattice parameter (nm)	c Lattice parameter (nm)	Cell volume (nm^3)
SnO_2	0.4739	0.3189	0.0716
$Sn_{0.75}Ti_{0.25}O_2$	0.4709	0.3136	0.0695
$Sn_{0.50}Ti_{0.50}O_2$	–	–	–
$Sn_{0.25}Ti_{0.75}O_2$	0.4638	0.3019	0.0649
TiO_2	0.4596	0.2960	0.0625

This was evidenced by the presence of a rutile single phase in SnO_2 and TiO_2 pure compositions and by $Sn_{0.75}Ti_{0.25}O_2$, $Sn_{0.25}Ti_{0.75}O_2$ binary compositions, and confirmed by the theoretical and experimental values of the unit cell volume (see Fig. 7 and Table 2). This means that the thermal process used in these compositions did not permit spinodal decomposition; secondary phases cannot be detected in less than 1% under X-ray resolution,

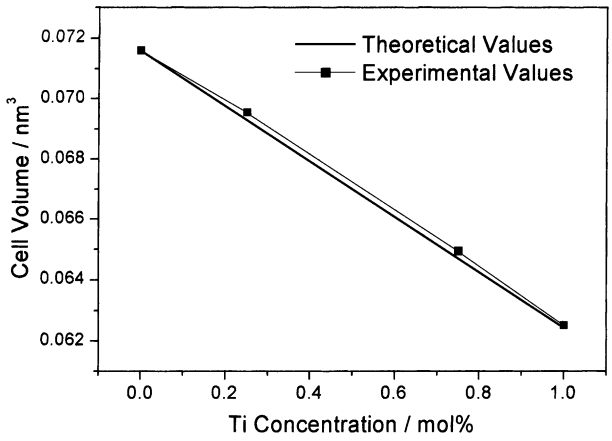

Fig. 7. SnO_2 unit cell volume as a function of the TiO_2 concentration. Experimental values obtained from Rietveld's method of structural refinement using the DBWS program.

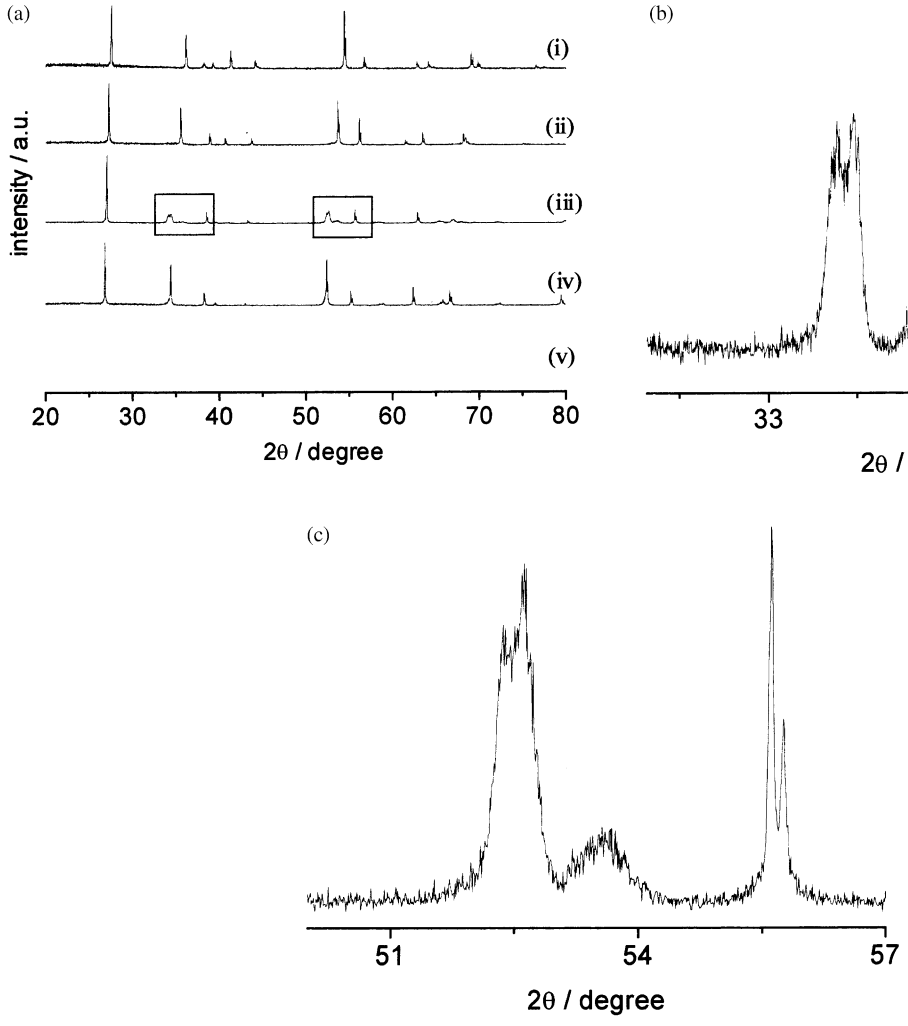

Fig. 6. X-ray diffraction patterns of pure and binary compositions: (a) (i) TiO_2; (ii) $Sn_{0.25}Ti_{0.75}O_2$; (iii) $Sn_{0.50}Ti_{0.50}O_2$; (iv) $Sn_{0.75}Ti_{0.25}O_2$; (v) SnO_2; (b) detail in the region of 30–40° (of 2θ) of $Sn_{0.50}Ti_{0.50}O_2$ composition; (c) detail in the region of 50–57° (of 2θ) of $Sn_{0.50}Ti_{0.50}O_2$ composition. Samples sintered at 1450 °C for 2 h in an ambient atmosphere, using a cooling rate of 10 °C min^{-1}.

although same secondary phase are seen by SEM micrographs (Figs. 3–5). Therefore, for the $Sn_{0.75}Ti_{0.25}O_2$ and $Sn_{0.25}Ti_{0.75}O_2$ materials, it could be affirmed that they do not undergo spinodal decomposition and a uniform solid solution is present in a great amount in these compositions, i.e., a major single phase of uniform composition is present when cooling begins and this phase is largely retained to room temperature. It should be noted that this was foreseen, since the kinetics of spinodal decomposition is quite slow[18–25] in $(Sn,Ti)O_2$ systems, varying strongly as aliovalent solutes that increase or decrease the extent of cation diffusion are added. Indeed, acceptor doping increases the rate of spinodal decomposition to the point where it is difficult to quench a solid solution without decomposition, whereas slight donor doping decreases the rate to the point where a sample can be annealed for many hours at 1000C without decomposing.[21]

As foreseen, spinodal phase precipitation clearly occurred in the $Sn_{0.50}Ti_{0.50}O_2$ sample (Figs. 4 and 6b and c), since the rate of spinodal decomposition is greatest when the compositions are close to $Sn_{0.50}Ti_{0.50}O_2$. Therefore, $Sn_{0.50}Ti_{0.50}O_2$ underwent spinodal decomposition and pure SnO_2 and TiO_2 phases were present in this sample. The spinodal decomposition of the $Sn_{0.50}Ti_{0.50}O_2$ solid solution gave rise to significant lattice distortion, which made it impossible to obtain the lattice parameter for this composition; hence, a lamellar structure can be seen (Fig. 4b) within each grain. Note that the microstructure of the $Sn_{0.25}Ti_{0.75}O_2$ binary composition (Fig. 5b) appears to show a small fraction of a decomposed phase in the grain boundary region (like a remanent liquid phase or a glass phase due to the spinodal decomposition), but was not detected as a new phase under X-ray refinement precision measurements, meaning it was lower than 1%. The difficult to X-ray refinement of $Sn_{0.50}Ti_{0.50}O_2$ is due to the fact that in spinodal decomposition the phase separation takes place in a manner that it is small in degree and large spatial extent. Therefore, some distortion of an expected X-ray pattern of a more common decomposition (such as nucleation and growth—that takes place in a manner that is large in degree but small in spatial extent) can be seen in Fig. 6b and c. These two different processes of decomposition a phase often result in different microstructures, especially at the earlier stages of phase separation (Fig. 4).

In an almost ideal solid solution between SnO_2 and TiO_2, the variation of enthalpy of the mixture is close to null. Hence, the following equation can be written for the cell volume of the system:

$$V_{SS} = X_{SnO_2} V_{SnO_2} + X_{TiO_2} V_{TiO_2} \quad (1)$$

where V_{SS} is the unit cell volume for the solid solution systems, and X_{SnO_2} and X_{TiO_2} are the mole fractions of SnO_2 and TiO_2, respectively. V_{SnO_2} and V_{TiO_2} are the unit cell volumes of SnO_2 and TiO_2, respectively. Fig. 7 shows the theoretical and experimental values of V_{SS} as a function of TiO_2 concentration in the binary compositions, indicating the formation of a solid solution in the $Sn_{0.25}Ti_{0.75}O_2$ and $Sn_{0.75}Ti_{0.25}O_2$ binary compositions.

Table 3 presents the mean grain size of the binary compositions obtained using image analysis software. The effect of the presence of TiO_2 was observed only in the $Sn_{0.25}Ti_{0.75}O_2$, which showed a significant increase in mean grain size (around 110%). The standard deviation showed that all the compositions obtained had a larger mean grain size distribution.

3.2. Sintering and densification rate

Fig. 8 depicts the linear shrinkage and linear shrinkage rate as a function of the temperature for pure SnO_2 and TiO_2. This fig. shows that the highest linear shrinkage of pure TiO_2 occurs close to 1000 °C. Fig. 8a shows that there is no linear shrinkage temperature for the pure SnO_2 sample, whereas the densifying mechanism of TiO_2 is activated around 1000 °C. The pure SnO_2 has no densifying mechanism in the temperature range studied in this work.

Linear shrinkage and linear shrinkage rate as a function of the temperature for binary compositions in Fig. 9 indicate that two mechanisms lead to densification in these systems, one activated at temperatures close to 1000 °C and the other activated at temperatures between 1200 and 1300 °C. SnO_2 doped with a concentration of MnO_2 and CoO under 1.5 mol% is single phase and, as demonstrated by Cerri et al.,[34] forms a substitutional solid solution. Cerri et al.[34] obtained relative densities around 99.0% for SnO_2–CoO and SnO_2–MnO_2 polycrystalline systems. The highest shrinkage rate occurred in the temperature range around 1100–1300 °C. Thus, modifying the SnO_2 lattice by the addition of CoO and MnO_2 caused a change in the densification rates and sintering mechanisms.

Cerri et al.[34] attributed the high densification to the increased concentration of oxygen vacancies in the grain boundary region. They proposed the following reactions for the formation of oxygen vacancies when SnO_2 is doped with MnO_2 and CoO in concentrations under 1.5 mol%:

Table 3
Mean grain size of the binary compositions

Compositions	Mean grain size (μm)	Median (μm)	Standard deviation (μm)
$Sn_{0.75}Ti_{0.25}O_2$	11.5	11.2	5.2
$Sn_{0.50}Ti_{0.50}O_2$	11.3	11.1	4.6
$Sn_{0.25}Ti_{0.75}O_2$	25.1	23.0	13.0
TiO_2	30.2	27.6	15.6

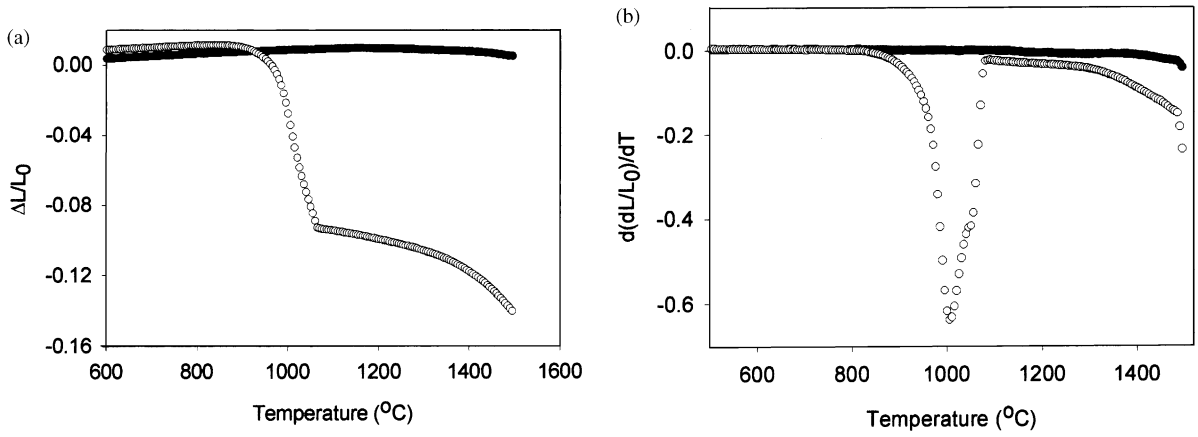

Fig. 8. Linear shrinkage (a) and linear shrinkage rate (b) as a function of temperature for pure SnO_2 and TiO_2: (Å) SnO_2 and (○) TiO_2. Heating rate of 10 °C min^{-1}.

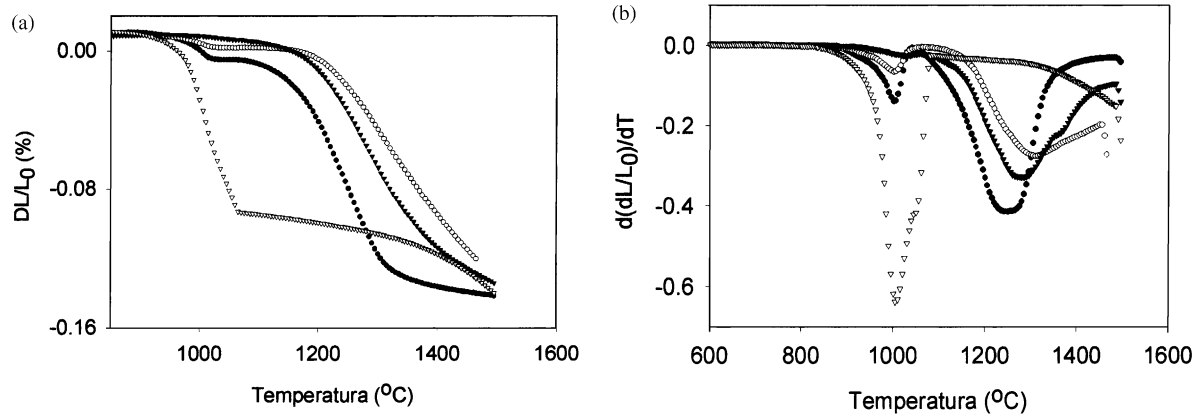

Fig. 9. Linear shrinkage (a) and linear shrinkage rate (b) as a function of temperature for SnO_2-TiO_2 compositions: (▼) $Sn_{0.75}Ti_{0.25}O_2$; (○) $Sn_{0.50}Ti_{0.50}O_2$; (Å) $Sn_{0.25}Ti_{0.75}O_2$ e (▽) TiO_2. Heating rate of 10 °C min^{-1}.

$$CoO \xrightarrow{SnO_2} Co''_{Sn} + V_O^{\bullet\bullet} + O_O^x, \quad (2)$$

$$MnO \xrightarrow{SnO_2} Mn''_{Sn} + V_O^{\bullet\bullet} + O_O^x. \quad (3)$$

Doping SnO_2 with MnO_2 and CoO leads to the creation of additional oxygen vacancies that increase the flux of oxygen ions and promote SnO_2 densification. These results are in agreement with the work of Yuan et al.,[35] who demonstrated that the Li^+ ion also promotes SnO_2 densification by increasing the flux of species that diffuse inside the material. Using TEM and Auger spectroscopy analyses, Gouvea[36] demonstrated that a liquid phase does not form during SnO_2 sintering with MnO_2, and that Mn^{+2} and Mn^{+3} ions are located near the grain boundaries (note that Mn^{+4} ions are reduced to Mn^{+2} and Mn^{+3} at high temperatures[34]). These results show that single-phase type sintering or solid state sintering occurs in SnO_2 doped with MnO_2.

The densifying mechanism in binary compositions at temperatures close to 1000 °C may be like the one in pure TiO_2, albeit occurring with a lower intensity. This densifying mechanism (mass transport mechanism) in pure TiO_2 may be related to the higher concentration of predominant defects such as double ionized oxygen vacancies and interstitial Ti^{4+} ions, at temperatures around 1000 °C, according to the electrical properties determined by Nowotny et al.[37] Nowotny et al.[37] concluded that the electrical properties involving electrical conductivity and thermo-power cannot be explained by a simple defect model, except under strongly reduced conditions. Moreover, they concluded that their electrical conductivity and thermo-power results should be considered in the light of several defects in comparable concentrations, such as Ti interstitials and Ti vacancies.

On the other hand, the densifying mechanism that is activated at temperatures between 1100 and 1300 °C may be similar to the one that occurred in the SnO_2–CoO and SnO_2–MnO_2 compositions studied by Cerri et al.[34] However, the Ti^{+4} ion has an ionic radius value of 0.68 Å while, in Sn^{+4}, the ionic radius value is 0.71 Å, and the substitution of Sn^{+4} by Ti^{+4} (or Ti^{+4} by Sn^{+4}) in the binary system lattice does not create oxygen vacancies

$$TiO_2 \xrightarrow{SnO_2} Ti_{Sn}^{x} + 2O_O^{x}, \quad (4)$$

such as MnO_2 and CoO doped SnO_2 [Eqs. (2) and (3)]. Therefore, while oxygen vacancies may be the main defects responsible for the densifying mechanism in SnO_2–CoO and SnO_2–MnO_2 systems, they are apparently not the only contributing factor for the densification in SnO_2–TiO_2 systems. Therefore, the above discussion disregards the creation of oxygen vacancy defects in SnO_2-TiO_2 systems by the addition of Ti atoms [Eq. (4)]. Oxygen vacancies as intrinsic defects may, however, be present in SnO_2–TiO_2 polycrystalline structures due to the fugacity of oxygen, which may increase the concentration of such defects at high temperatures. Under such conditions, the reduction of the valence state of Sn^{+4} atoms to the Sn^{+2} state could give rise to charge compensation. In other words, the oxygen fugacity cannot be disregarded in this case and can also contributing to the second mass transport mechanism.

The subject of solid state defect chemistry has been considerably debated in the literature insofar as it concerns oxygen vacancy vs. titanium interstitial models for point defect diffusion in rutile TiO_2, and Henderson's recent work[38] concerning self-diffusion in rutile TiO_2 elucidates the subject. Henderson's[38] results, obtained by static secondary ion mass spectroscopy using isotopic enrichment of ^{18}O and ^{46}Ti surfaces, strongly suggest that subsurface diffusion of reduced titanium cations is the mechanism by which ion-sputtered TiO_2 single crystal surfaces are re-oxidized by the bulk during annealing in an ultrahigh vacuum, suggesting that Ti interstitials are the major diffusive species in TiO_2 rutile and not O atoms/vacancies. The sputtered TiO_2 (110) surface remains heavily reduced at temperatures lower than 400 K (~125 °C), but the O/Ti ratio increases slowly above 400 K and rapidly above 700 K (425 °C).

Henderson's results also show that no diffusion is detected between the surface and bulk at temperatures under 400 K; however, diffusion of both oxygen and titanium are detected between 400 and 700 K without any significant change in the surface stoichiometry. Above 700 K, only titanium diffusion from the surface to the bulk is detected.

The chemical diffusion results reported by Radecka et al.[31] suggest that the above statements may also be valid for $(Sn,Ti)O_2$ systems. The coefficient of chemical diffusion of $(Sn,Ti)O_2$ compositions was found to be independent of partial oxygen pressure. In addition, when these chemical diffusion coefficients are compared with those of the pure TiO_2 composition, the addition of Sn to TiO_2 appears to decrease diffusivity (Fig. 8).

Our results are in agreement with the work of Radecka et al.[31] The higher the TiO_2 concentration in the mixture, the higher the system's relative density and, hence, the higher its densification during sintering. Moreover, the system's mean grain size increases when the SnO_2 concentration decreases in the TiO_2 lattice (when TiO_2 is present in concentrations above 50 mol%). In other words, binary compositions acquire increasingly pure TiO_2 sintering features as the TiO_2 content is increased.

Radecka et al.[31] also concluded that mass transport across the grain boundary of $(Sn,Ti)O_2$ compositions is very fast and that the kinetics is determined by mass transport diffusion from the grain boundary into the bulk phase, i.e., diffusion at the grain boundary is the mechanism responsible for total mass transport. This conclusion is also in agreement with the mean grain size results shown in Table 3 and with Henderson's conclusions.[38]

Fig. 9 shows that the intensity of each densifying mechanism depends on the SnO_2 or TiO_2 concentration. Hence, TiO_2 is the main component responsible in the first mechanism (temperatures around 1000 °C) proposed above. This conclusion is illustrated by a comparison of Figs. 8 and 9. When TiO_2 concentrations decrease, the mass transport related to the mechanism around 1000 °C also decreases. On the other hand, decreasing the TiO_2 fraction causes the contribution of SnO_2 to densification to increase at temperatures of 1100–1300 °C. An analysis of the linear shrinkage rate as a function of the temperature of the $Sn_{0.50}Ti_{0.50}O_2$ composition also shows that the spinodal decomposition influences the second mass transport mechanism between 1100 and 1300 °C, modifying the tendency observed in the other compositions.

Based on the above evidence, we have assumed that the first mechanism for mass transport in SnO_2–TiO_2 systems, which is present at 1000 °C, is governed mainly by diffusion of the interstitial titanium atom and Ti vacancies, while the second mechanism, occurring at temperatures between 1100 and 1300 °C is unclear, maybe associated with faster grain boundary diffusion caused by oxygen vacancies in the SnO_2–TiO_2 due to fugacity. Since SnO_2 and TiO_2 share a common structure and, thus, a common oxygen sublattice, the diffusivity in this binary system requires a mixture of both major densifying mass transport mechanisms that are present in each TiO_2 pure component and CoO- and MnO_2-doped SnO_2 (mainly the densifying mass transport mechanism in SnO_2 systems). The presence of diffusivity of oxygen vacancies in SnO_2–TiO_2 systems at higher temperatures can be inferred based on an interpretation of Eq. (5) that will be discussed later.

A discussion of the chemical potential may also help to better understand the presence of the two densification mechanisms (mass transport) in the $(Sn,Ti)O_2$ system. SnO_2 has strong covalent and ionic characteristics such as crystalline SiO_2. Pure crystalline solids, containing primarily covalent chemical bonds, are rarely densified during sintering without the application of pressure.[39] On the other hand, TiO_2 is a primarily ionic

crystalline solid. Thus, higher concentrations of TiO_2 in the mixture should produce stronger ionic bonding characteristics in the $(Sn,Ti)O_2$ binary system, leading to greater densification during sintering as a result of higher and faster mass transportation by ionic diffusion.

It is common for the chemical potential to change as a result of an alteration in the nature of a chemical bond in a mixture. TiO_2 densifies without the need for dopants in the lattice because it possesses a mechanism for mass transport that produces densification, while pure SnO_2 has no densification mechanism. The mass transport mechanism in pure SnO_2 occurs by surface diffusion at temperatures below 800 °C; above that temperature, the main mass transport mechanism is evaporation-condensation, a non-densifying mechanism.[14] This mechanism is triggered by the easy evaporation of SnO_2 at high temperatures, as illustrated in Eq. (5)

$$SnO_{2(s)} \rightarrow SnO_{(g)} + 1/2O_{2(g)}. \quad (5)$$

The chemical bonding nature of SnO_2 is also more covalent than that of TiO_2. Crystalline solids containing primarily covalent chemical bonds are "unsinterable", i.e., no extensive macroscopic shrinkage (densification) of the powder compact occurs during heat treatment without the application of pressure.[39] This difference between the bonding nature of pure SnO_2 and TiO_2 oxides implies difficult ionic diffusion in SnO_2 and the existence of a non-densifying mass transport mechanism (hence, low self-diffusion coefficients). The explanations for this lack of sintering in solids with directional and high covalent bond characteristics involve both kinetic and thermodynamic considerations. However, in the absence of sufficient experimental data, certain authors[40] believe that the activation energy required for self-diffusion is extremely high because of the large amount of energy required for the formation and motion of structural defects in solids having directional covalent bonds.

The addition of TiO_2 to the SnO_2 lattice, with the development of a substitutional solid solution, should modify the nature of the mixture's chemical bond and chemical properties and, therefore, the mechanism for mass transport discussed earlier herein. In other words, the solid solution can be the driving force to densification. The evaporation–condensation mechanism decreases and a mechanism for mass transport through grain boundary diffusion, for example, just as in pure TiO_2 (the mass transport mechanism existing at 1000 °C), must appear. This would naturally lead to densification of the $(Sn,Ti)O_2$ systems. However, the mass transport mechanism that occurs in SnO_2–TiO_2 compositions at temperatures between 1100 and 1300 °C cannot be described by a recognized mechanism or be attributed to a certain defect in the absence of more experimental data.

4. General discussion

As mentioned earlier herein, Cerri et al.[34] suggested that low MnO and CoO concentrations promote SnO_2 densification by increasing the concentration of oxygen vacancies, which in turn increases the role of mass transport through the grain boundary. However, as discussed previously, it would be inaccurate to state that this same behavior is the sole mass transport mechanism in the binary composition studied here. Other factors, such as interstitial defects, also cause increased mass transport, according to Radecka et al.,[31] Henderson,[38] and Yuan and Virkar[21] and the second mass transport mechanism is not clear, but probably are related to mass transport through the grain boundary.

Mass transport in binary compositions can be discussed from two different standpoints, i.e., SnO_2 or TiO_2 mass transport. From the standpoint of SnO_2, the mass transport mechanism changes when TiO_2 is present in the SnO_2 lattice. In other words, sintering mechanisms are altered when SnO_2 is doped or mixed with TiO_2 and the solid state solution is one of the driving forces contributing to the total mass transport. In pure SnO_2, a non-densifying mechanism such as evaporation–condensation, is predominant, though inactive in the SnO_2–TiO_2 mixture. However, in this mixture, a new mass transport mechanism may arise, such as mass transport through the boundary, which can lead to a higher self-diffusion and/or oxygen vacancy diffusivity for example.

The binary compositions studied here are particularly relevant for a better understanding of mass transport mechanisms during sintering in ceramic systems in general. These binary compositions are even more important because they show two clearly distinct regions of linear shrinkage (Fig. 9), which indicate the simultaneous existence of two mass transport mechanisms. This characteristic can be used to obtain different degrees of densification. An in-depth study to quantify the contribution of each mechanism to the overall densification of all compositions would also be relevant.

The literature contains few reports regarding SnO_2–TiO_2 binary properties. The reports on findings regarding these systems deal with the kinetics of spinodal decomposition,[20–25] as stated in the introduction. Several important applications should emerge from these binary systems due to the vast number of potential applications of pure SnO_2 and TiO_2 components. One possible application was discussed by Radecka et al.,[30] who analyzed the SnO_2–TiO_2 binary systems for H_2 sensor applications. Resistance as a function of partial H_2 pressure showed great reproducibility, which is a very important factor in such applications. Small amounts of TiO_2 in SnO_2–TiO_2 systems improve sensor performance and increase the detection interval to 10,000 ppm of H_2 (previously it had ranged from 500 to

1000 ppm of H_2).[31] Higher TiO_2 concentrations decrease sensor performance owing to decreased surface areas. Radecka et al. also suggested that the addition of TiO_2 promotes an increase of surface density centers, activated for chemisorption, when added in the $(Sn_x,Ti_{1-x})O_2$ system.

We also verified the optimal performance of an $(Sn,Ti)O_2$ binary composition for other applications compared to a pure SnO_2 and TiO_2 composition. Several preliminary experiments have been carried out in our laboratory to study the properties of SnO_2–TiO_2 and some of our findings show that these systems are promising for electrochemical (electrocatalysis) and sensor applications.

5. Conclusions

The $(Sn,Ti)O_2$ systems showed high density after sintering. Two mass transport mechanisms contributing to densification were observed in these systems. The more TiO_2 contained in the system, the greater its densification.

Our studies of the sintering mechanisms of these binary systems have brought to light two mass transport mechanisms. We believe our findings can be relevantly applied for a better understanding of sintering and mass transport in other oxide systems.

Acknowledgements

The support of this work by the Brazilian research funding institution FAPESP is gratefully acknowledged.

References

1. Jarzebski, J. M. and Marton, J. P., *J. Electrochem. Soc*., 1976, **123**, 199C.
2. Jarzebski, J. M. and Marton, J. P., *J. Electrochem. Soc*., 1976, **129**, 299C.
3. Fagan, J. F. and Amarakoon, V. R. W., *Am. Ceram. Soc. Bull*., 1993, **72**, 119.
4. Chopra, K. L., Major, S. and Pandya, P. K., *Thin Solid Films*, 1983, **102**, 1.
5. Duhn, J. G., Jou, J. W. and Chiou, B. S., *J. Electrochem. Soc*., 1989, **136**, 2740.
6. Semancik, S. and Fryberg, T. B., *Sensor & Actuators B*, 1990, **1**, 97.
7. Göpel, W. and Shierbaum, K. D., *Sensor & Actuators B*., 1995, **26**, 1990.
8. Seiyama, T., Yamazae, N. and Arai, H., *Sensor & Actuators B*, 1983, **4**, 85.
9. Ihokura, K., Tanaka, K. and Murakami, N., *Sensor & Actuators B*, 1983, **4**, 612.
10. Pianaro, S. A., Bueno, P. R., Longo, E. and Varela, J. A., *J. Mat. Sci. Lett*., 692, **14**, 1995.
11. Traversa, E., *J. Am. Ceram. Soc*., 1995, **78**, 2625.
12. Park, S. J., Hirota, K. and Yamamura, H., *Ceram. Inter*, 1984, **10**, 116.
13. Islam, M. H. and Hogarth, C. A., *J. Mat. Sci. Lett*., 1989, **8**, 986.
14. Panteleev, V. G., Ramm, K. S. and Pronkina, T. I., *Steklo i Keramica*, 1989, **5**, 18.
15. Finklea, H. O., *Semiconductor Electrodes*. Elsevier, Amsterdam, 1988.
16. Yan, M. F. and Rhodes, W. W., Appl. *Phys. Lett*., 1982, **40**(6), 536–537.
17. Schultz, A. H. and Stubican, V. S., *Philos. Mag*, 1968, **18**, 929–937.
18. Stubican, V. S. and Shultz, H., *J. Am. Ceram. Soc*., 1970, **53**(4), 211–214.
19. Gupta, P. K. and Cooper, A. R., *Philos. Mag*, 1970, **21**, 611–617.
20. Park, M., Mitchell, T. E. and Heuer, H., *J. Am. Ceram. Soc*., 1975, **58**, 43–47.
21. Yuan, T. C. and Virkar, A. V., *J. Am. Ceram. Soc*., 1988, **71**(1), 12–21.
22. Flevaris, N. K., *J. Am. Ceram. Soc*., 1987, **70**(5), 301–304.
23. Wu, K. and Mendelson, K. S., *J. Chem. Phys*., 1975, **58**(1), 43–47.
24. Virkar, A. V. and Plichta, M. R., *J. Am. Ceram. Soc*., 1983, **66**(6), 451–456.
25. Nambu, S., Sato, A. and Sagala, D. A., *J. Am. Ceram. Soc*., 1992, **75**(7), 1906–1913.
26. Cahn, J. W., *Acta Met*, 2001, **9**(9), 795–801.
27. Rundman, K. B. and Hillard, J. E., *Acta Met., 15,* -, 1025, **1033**, 1967.
28. Woodilla, J. E. Jr. and Averbach, B. L., *Acta Met*., 1968, **16**, 255–263.
29. Tomazawa, M., MacCrone, R. K. and Herman, H., *J. Am. Ceram. Soc*., 1970, **53**(1), 62–63.
30. Radecka, M., Zakrzewska, K. and Rekas, M., *Sensor & Actuators B*, 1988, **47**, 194–204.
31. Radecka, M., Zakrzewska, K. and Rekas, M., *Solid State Ionic*, 1999, **119**, 43–48.
32. Rietveld, H. M., *Acta Cryst*, 1967, **22**, 151–152.
33. Young, R. A., Sakthiveli, T. S., Moss, C. and Pava–Santos, O., *J. Appl. Cryst*, 1995, **28**, 366–367.
34. Cerri, J. A., Leite, E. R., Gouvêa, D., Longo, E. and Varela, J. A., *J. Am. Ceram. Soc*., 1996, **79**, 799–804.
35. Yuan, D. W., Wang, S. F., Huebner, W. and Simkovich, G., *J. Mater. Res*., 1993, **8**, 1975–1979.
36. Gouvêa, D. Thesis, Federal University of São Carlos, 1996.
37. Nowotny, J., Radecka, M. and Rekas, M., *J. Phys. Chem. Solids*, 1997, **58**(6), 927–937.
38. Henderson, M. A., *Surface Science*, 1999, **419**, 174–187.
39. Greskovich, C. and Rosolowski, J. H., *J. Am. Ceram. Soc*., 1976, **59**, 336–343.
40. Bron, V. A., *Sov. Powder Metall. Met. Ceram*, 1972, **5**, 339–344.